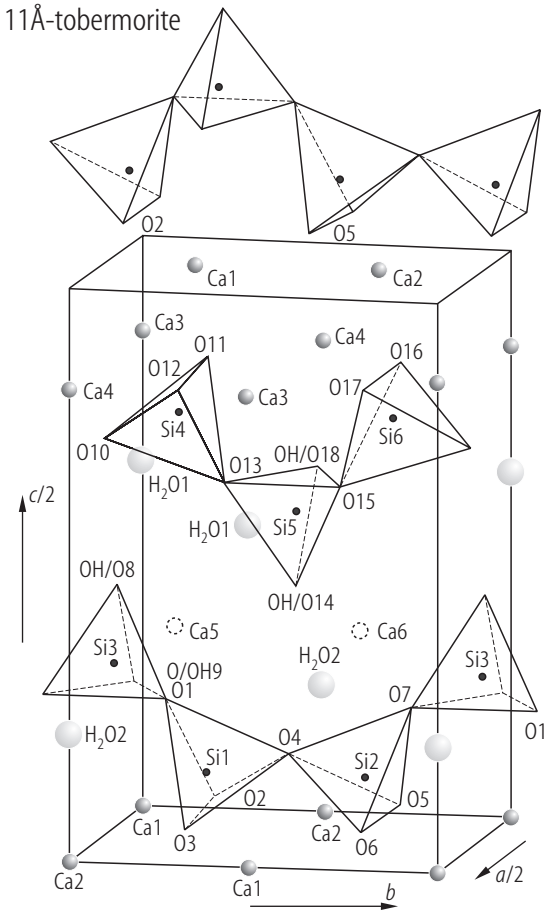

←

Fig. 1. 11Å-tobermorite. Orthorhombic lattice (1/8 of the cell with $a/2$ = 5.58 Å, b = 7.39 Å, $c/2$ = 11.389 Å). The labile calcium ions (dashed circles) are statistically spread between sites Ca5 and Ca6, the Ca1 to Ca4 sites being occupied by the non-labile calcium ions [81H1].

Fig. 2. Tobermorites. **(a)** Clinotobermorite, columns of CaO_7 polyhedra, schematically represented as trigonal prisms completed by the "capping" ligands. Two adjacent columns are drawn (displaced along the dashed lines) to show the polyhedral connection [00M1]. **(b)** Silicate double chains in: (**b1**) xonotlite [79K1], (**b2**) clinotobermorite [00M1] and (**b3**) 11Å-tobermorite [99M1]. The double chains are projected along the chain direction and perpendicular to it, respectively [00M1].

↓

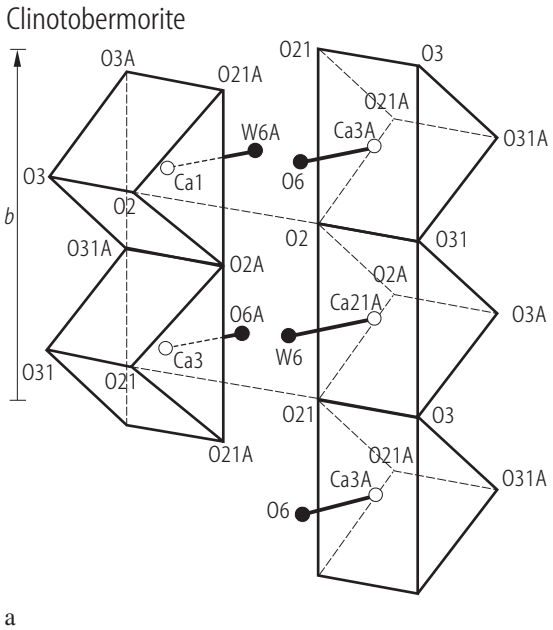

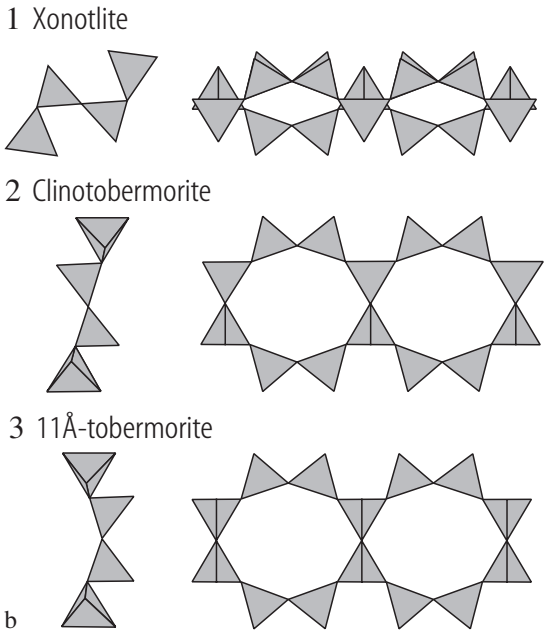

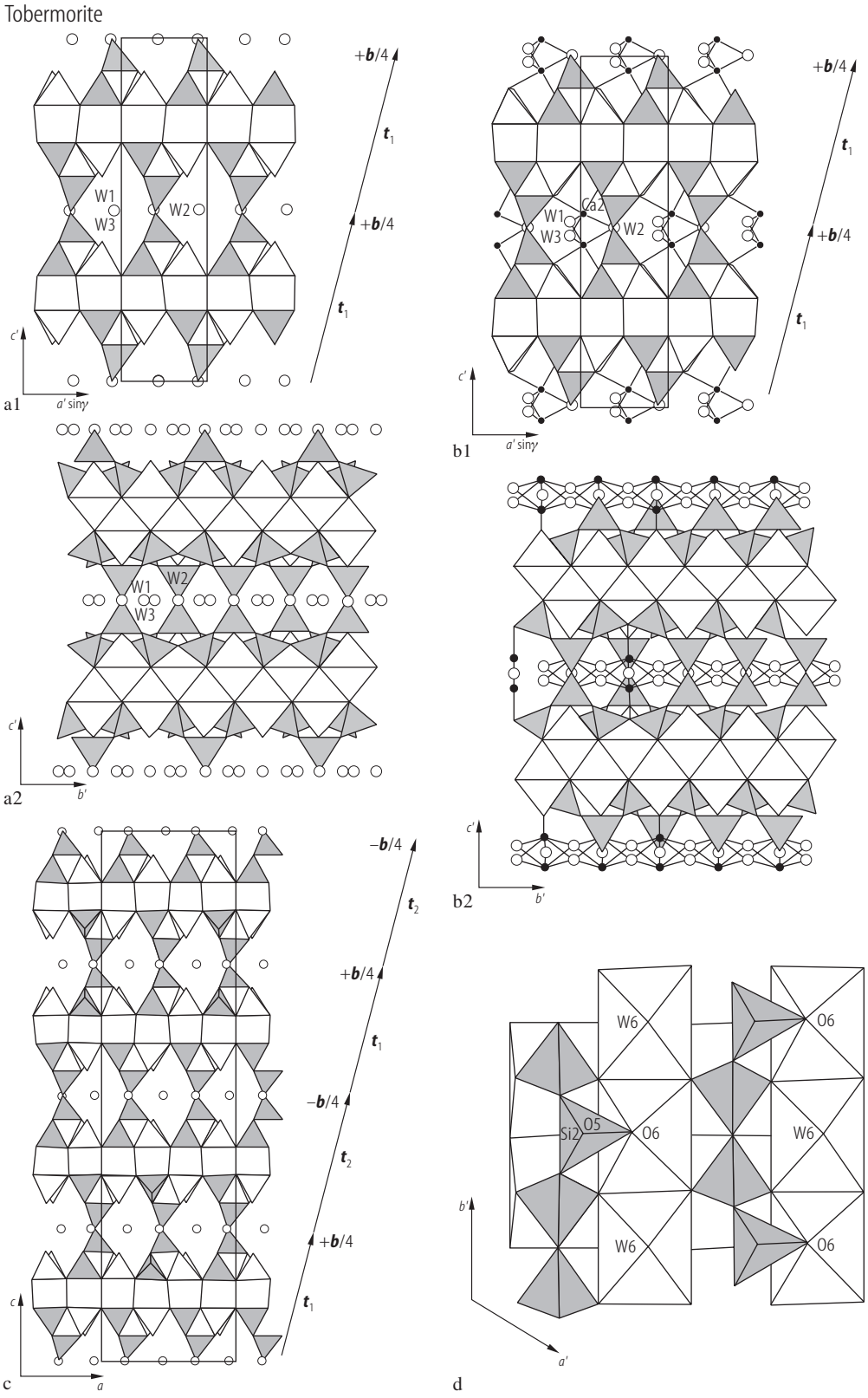

Fig. 3. For caption see next page

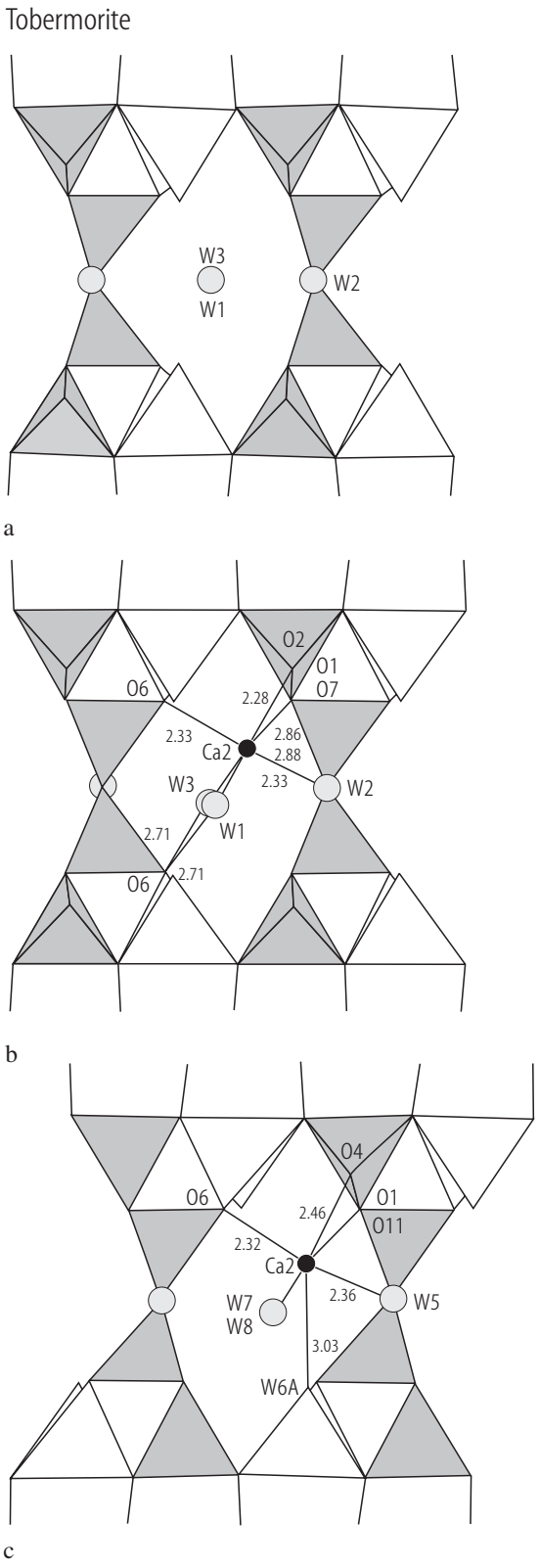

↑ (Fig. 3 see previous page)

Fig. 3. Tobermorites. Crystal structures: (**a**) monoclinic polytype MDO_2 of anomalous 11Å-tobermorite as seen along [010] (**a1**) and down [210] (**a2**). Silicate double chains (grey) are connected to layers of sevenfold coordinated Ca polyhedra. Open circles indicate the "zeolitic" water molecules W1, W2 and W3. The stacking vectors are drawn in (a1) with the indication of their component along ***b***; (**b**) monoclinic polytype MDO_2 of normal 11Å tobermorite, as seen along [010] (**b1**) and down [210] (**b2**). Black dots indicate additional calcium cations Ca2; (**c**) orthorhombic polytype MDO_1 as seen along [010]; (**d**) connection of silicate chains (grey) to the layer of calcium polyhedra as seen along [001] [01M1].

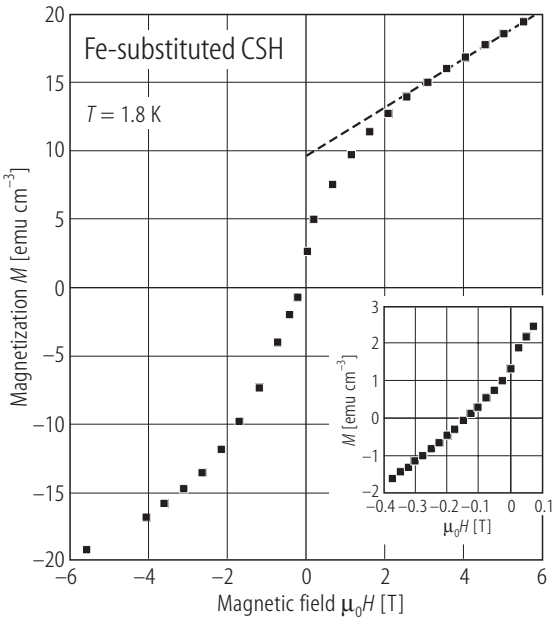

Fig. 5. Fe-substituted CSH. Magnetization isotherm at 1.8 K. Inset: the weak magnetization range showing the coercive field [97L1].

←

Fig. 4. Tobermorites. Schematic drawing of the structural cavities as seen along [010] in: (**a**) anomalous 11Å-tobermorite (Wessels mine); (**b**) normal 11Å-tobermorite (Ural mine); (**c**) clinotobermorite (Wessels mine) [00M1, 01M1]. In (**b**) one of the two possible ordered arrangements of Ca2, W1 and W3 are shown.

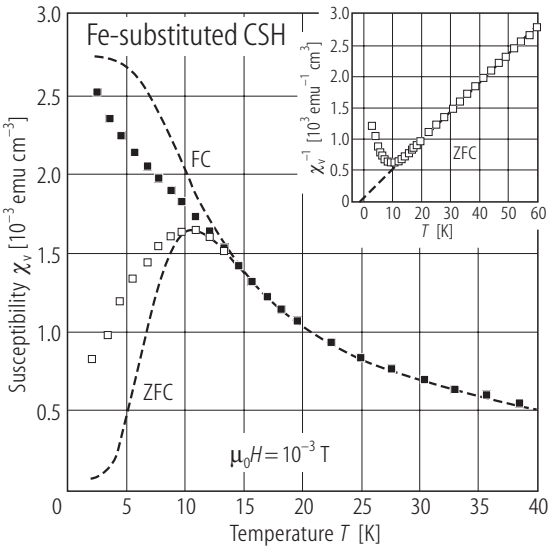

Fig. 6. Fe-substituted CSH. Low-field ZFC and FC susceptibilities. The dashed lines are theoretical calculations using a model of non-interacting particles and assuming a log-normal particle size distribution with d_o = 5 nm and σ = 0.1 and with anisotropy constant K = 4.4·10^5 erg/cm^3 and M_o = 10 emu/cm^3. In inset the inverse ZFC susceptibility as a function of temperature is shown. The dashed line is a Curie-Weiss law with Θ = –1.6 K [97L1].

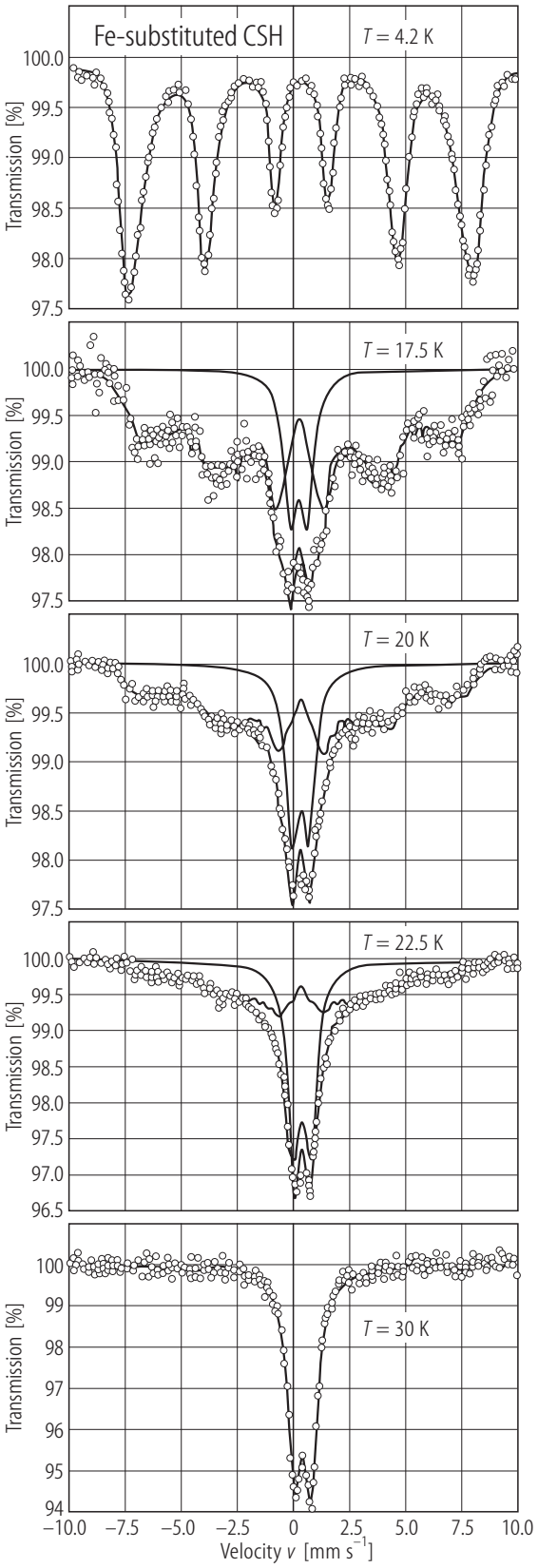

→

Fig. 7. Fe-substituted CSH. ^{57}Fe NGR spectra at 4.2 K ≤ T ≤ 30 K. Except at 4.2 K and 30 K, the solid lines shows the decomposition into two spectra components (a distribution of magnetic hyperfine patterns and a quadrupole doublet), characteristic of an ensemble of superparamagnetic small particles [97L1].

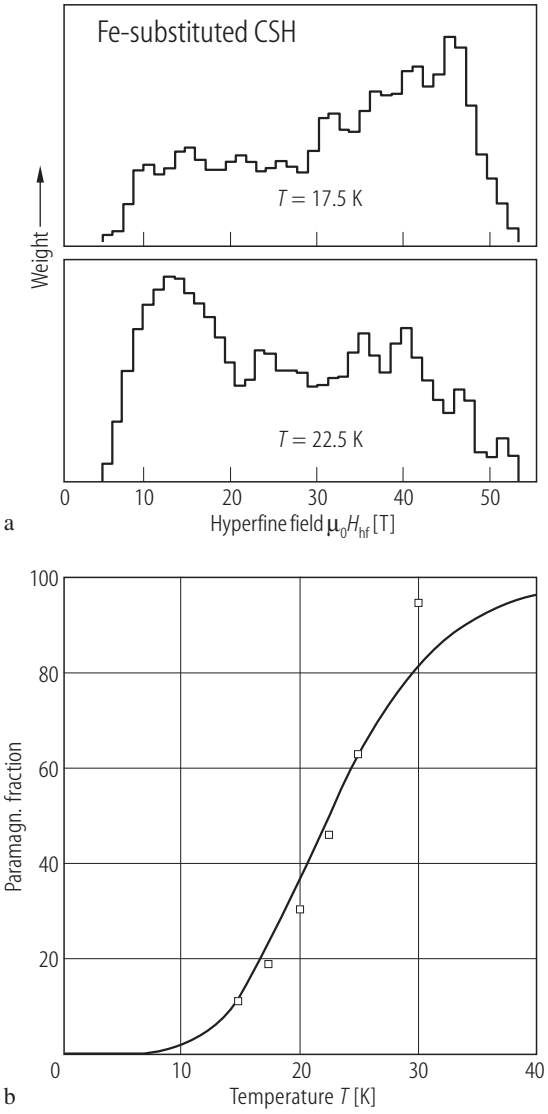

Fig. 8. Fe-substituted synthetic CSH. **(a)** Histograms describing the hyperfine field distribution of the magnetic hyperfine component in the ^{57}Fe NGR spectra at 17.5 K and 22.5 K. **(b)** Thermal variation of the relative percentage of the quadrupole doublet (rapidly fluctuating particles). The solid line is a fit using a log-normal particle size distribution with d_o = 5 nm, σ = 0.1 and $K = 4.4 \cdot 10^5$ erg/cm^3 [97L1].

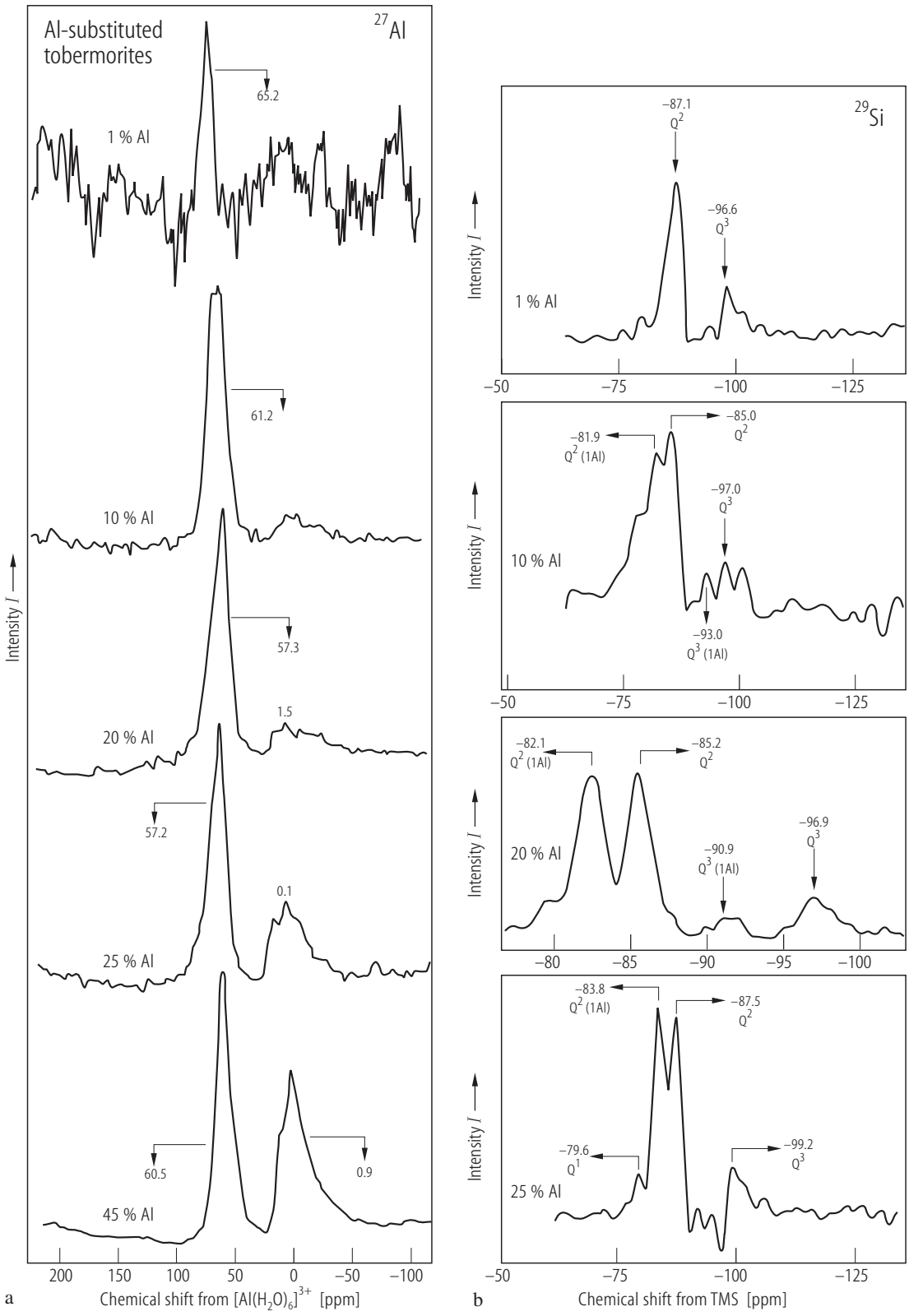

Fig. 9. Al-substituted tobermorites. **(a)** ^{27}Al MAS NMR spectra; **(b)** ^{29}Si MAS NMR spectra [91T1].

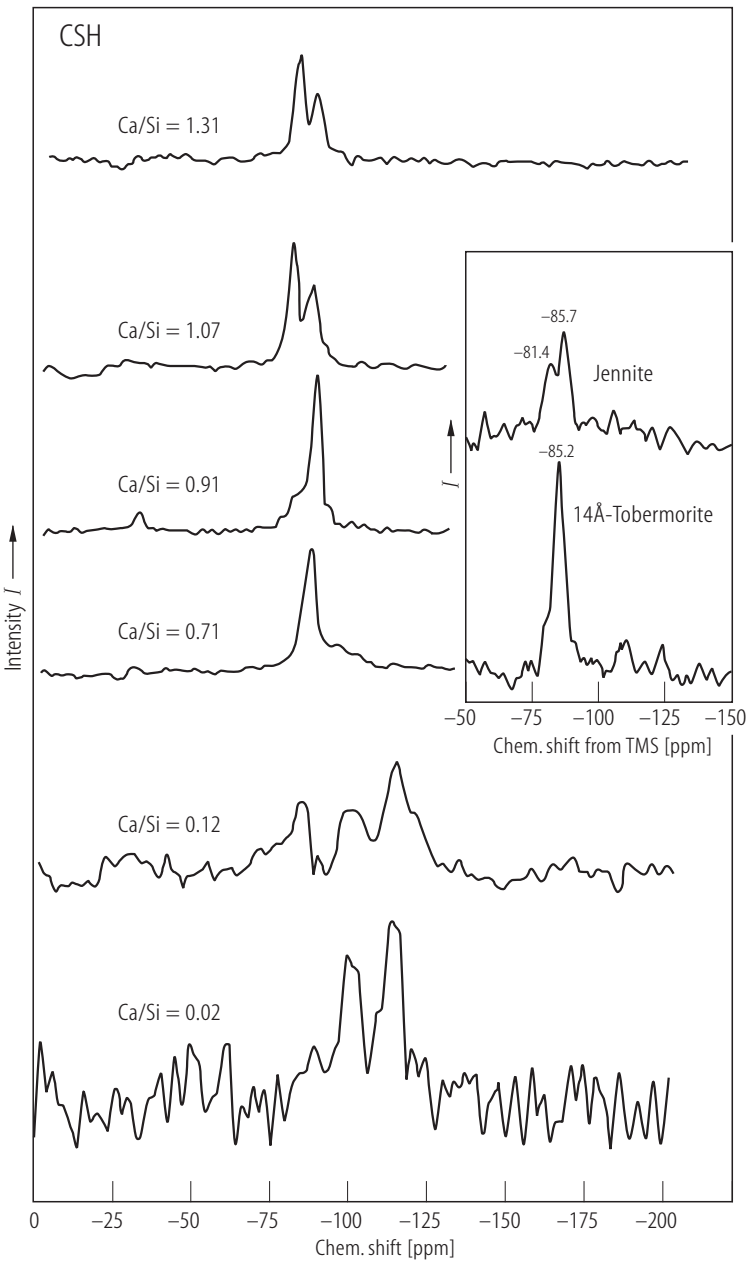

Fig. 10. Calcium silicate hydrates. ^{29}Si MAS NMR spectra [89G1]. The spectra of jennite and 14Å-tobermorite are also shown in inset. Chemical shifts are relative to TMS.